Electronic Supplementary Material (ESI) for Energy & Environmental Science

Supporting Information

Effective Nonmetal Incorporation in Black Titania with Enhanced Solar Energy Utilization

Tianquan Lin,[1,2] Chongyin Yang,[1,2] Zhou Wang,[1,2] Hao Yin,[1] Xujie Lü,[1] Fuqiang Huang,[1,2,*] Jianhua Lin,[2] Xiaoming Xie,[3] and Mianheng Jiang[3]

[1] CAS Key Laboratory of Materials for Energy Conversion, Shanghai Institute of Ceramics, Chinese Academy of Sciences, Shanghai 200050, P.R. China;
[2] College of Chemistry and Molecular Engineering, Peking University, Beijing 100871, P.R. China;
[3] State Key Laboratory of Functional Materials for Informatics, Shanghai Institute of Microsystem and Information Technology, Chinese Academy of Sciences, Shanghai 200050, P.R. China.

Content

1. The formation mechanism of black TiO_{2-x}

Plenty of oxygen vacancies are first introduced in TiO_2 nanocrystals to obtain oxygen-deficient titania (TiO_{2-x}) by the reduction of melted Al in an evacuated two-zone furnace. More efficient reduction can be achieved in our Al-reduced sample than the H_2-reduced samples previous report, consistent with Ellingham diagram shown in Figure S1. The Ellingham diagram used to show the conditions under which a metal oxide can be reduced to a metal. The standard Gibbs free energy of formation of the oxide is considered, for example, $M+\frac{1}{2}O_2 \rightarrow MO$. This value, $\Delta G^{\ominus}$, is plotted against temperature. The straight lines in the Ellingham diagram (Figure S1) represent the function ΔG^0 (T) and the relative stability of oxides. It is possible to visualize directly the affinities of metals for oxygen in their standard conditions by observing the relative positions of the lines in the diagram. A given metal can reduce the oxides of all other metals whose lines lie above theirs on the diagram. For example, the $2Ti_2O_3 + O_2 \rightarrow 4TiO_2$ line lies above $4/3Al + O_2 \rightarrow 2/3Al_2O_3$ line but below the $H_2 + O_2 \rightarrow H_2O$ line, so elemental Al can reduce TiO_2 to Ti_2O_3 but H_2 cannot at low temperature.

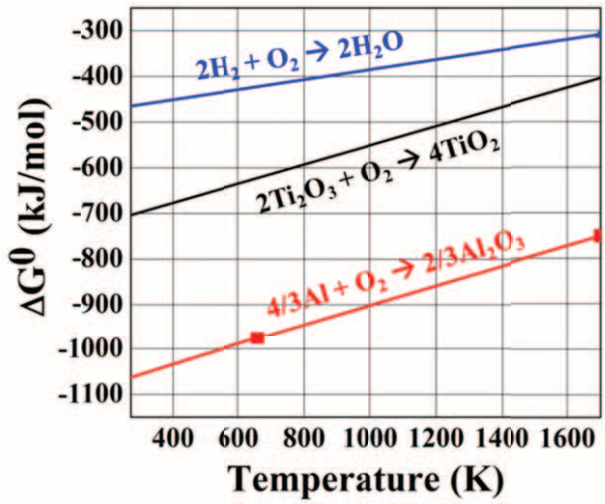

Figure S1. Ellingham diagram of ΔG versus temperature.

It is a convenient way to obtain the equilibrium oxygen partial pressure at a given temperature using the following equation:

$$\Delta G^0 = -RT \ln p_{O_2}$$

Any combination of values (ΔG^0, T) in the diagram represents a particular value of oxygen partial pressure. If the oxygen partial pressure is higher than the equilibrium value, the metal will be oxidized; in contrast, if it is lower than the equilibrium value then the oxide will be reduced. In this research, the melted Al at 800 °C can effectively decrease oxygen partial

pressure. When the oxygen partial pressure of TiO_2 is much lower than its equilibrium value, the TiO_2 is readily reduced.

2. Preparation of *X*-doped TiO_2 (*X*=N, S, I) following the literature methods

The N-doped TiO_2 (N:TiO_2) was prepared according to previously reported procedure.[S1] Typically, the commercial TiO_2 (Degussa P25) powder were treated at 600 °C under a NH_3 (67%)/Ar gas flow at 1 atm for 3 h.

The S-doped TiO_2 (S:TiO_2) sample was prepared according to the following procedure.[S2] At 40 °C, a solution containing 10 mL ethanol and 2.5 mL dilute HNO_3 aqueous solution (20%) was added into a solution containing 40 mL ethanol and 10 mL $Ti(O\text{-}C_4H_9)_4$ under vigorous stirring. After being aged for 24 h at 40 °C, the as-prepared TiO_2 xerogel was transferred into a 100 mL autoclave containing 25 mLCS_2/EtOH solution and was heated slowly to 240 °C for 2 h. The solid was then further calcined at high temperature for 8 h to remove the residual organic compounds to obtained S-doped TiO_2 (S:TiO_2).

The I-doped TiO_2 (I:TiO_2) sample was prepared according to previously reported method.[S3] In the typical procedure, 2.5 g $Ti(SO_4)_2$ was dissolved in potassium iodate (KIO_3, 0.05mol/L) under stirring. The resultant white slurry was transferred to a Teflon-lined autoclave and reacted at 100°C for 24 h. The resultant yellow powder was centrifuged, washed with deionized water, followed by calcination at 300 °C for 2 h.

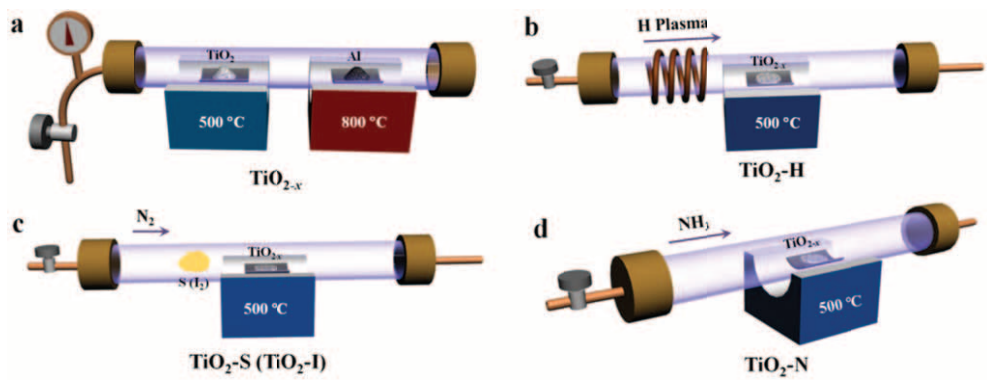

Figure S2. The equipment schematics of preparation samples. (a) Schematic low-temperature reduction of TiO_2 (TiO_{2-x}) in a two-zone furnace. (b) Preparation of H-doped black titania (TiO_2-H) in a thermal plasma furnace by hydrogen plasma. (c) Preparation of S- and I-doped black titania (TiO_2-S, I) by the reaction of the as-prepared TiO_{2-x} with S and I_2 atmosphere at 500 °C for 4 h, respectively. (d) Preparation of N-doped black titania (TiO_2-N) by heat treatment of TiO_{2-x} powder at 500 °C for 4 h with a NH_3:Ar=2:1 gas flow.

The color of TiO_2-X sample varies with the doping element of X (H, N, S, I). For comparison, the photos of all the titania samples (including pristine TiO_2, TiO_{2-x}, TiO_2-H, TiO_2-N, TiO_2-S, TiO_2-I, H:TiO_2, N:TiO_2, S:TiO_2, and I:TiO_2) was provided in Figure S3.

Figure S3. The photos of all the titania samples (including pristine TiO_2, TiO_{2-x}, TiO_2-H, TiO_2-N, TiO_2-S, TiO_2-I, H:TiO_2, N:TiO_2, S:TiO_2, and I:TiO_2) for comparison.

3. XRD patterns, HRTEM images and elemental abundances of titania samples

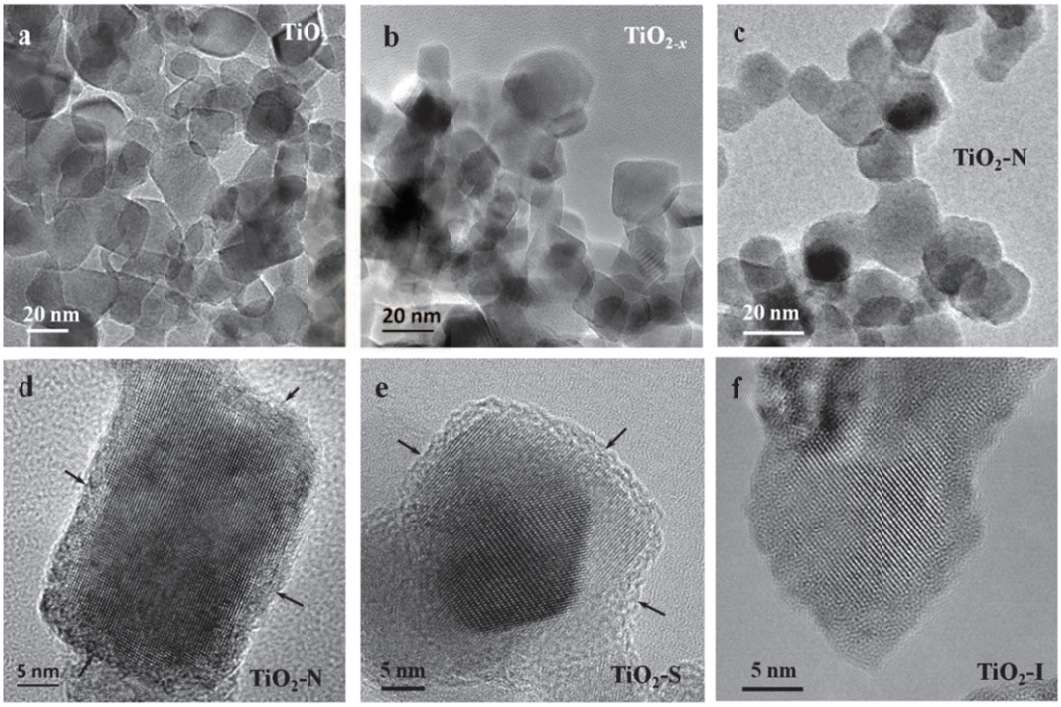

Figure S4. (a–f) TEM image and HRTEM images of pristine TiO_2, TiO_{2-x} and nonmetal-doped TiO_2, respectively. These nanocrystals are averagely ~25 nm in diameter.

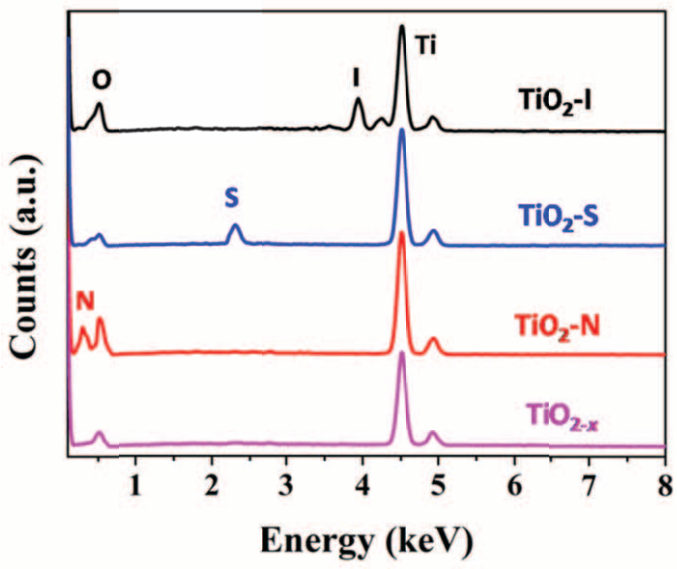

Figure S5. Energy dispersive spectroscopic (EDS) spectra of TiO_{2-x} and T**i**O_2-*X* (*X*=N, S, I), confirming the existence of nonmetal elements in the nonmetal- doped black titania.

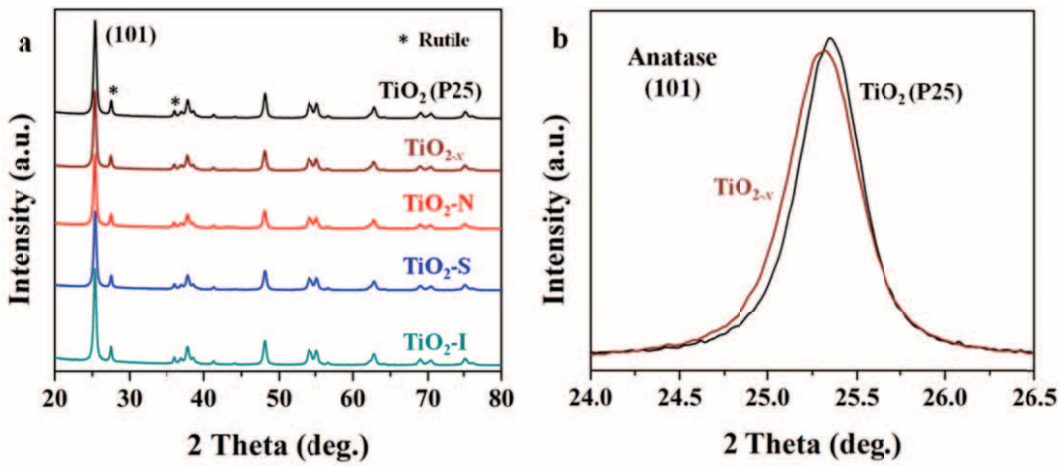

Figure S6. (a) XRD patterns of TiO_2 before and after the Al reduction and TiO_2-*X* (*X* = N, S, I). (b) Enlarged view of the (101) XRD peak of anatase. The strong diffraction peaks indicate that pristine TiO_2 (Degussa P25, a mixture of anatase and rutile), black TiO_{2-x} and nonmetal-doped TiO_2-*X* (*X* = N, S, I) remain high crystallinity. Nevertheless, the black TiO_{2-x} exhibits a larger linewidth than pristine TiO_2, which is derived from oxygen vacancies, as-resulted disorder-induced lattice strains.

The nonmetal element contents in titania samples were observed in the X-ray photoelectron spectroscopy (XPS) measurements, as listed in Table S1 and shown in Figure S7.

Table S1. Elemental abundances determined by XPS in titania samples.

Samples	Ti	O	N	S	I
TiO_2 (P25)	27.85	72.3	-	-	-
TiO_{2-x}	28.1	70.8	-	-	-
TiO_2-N	27.65	65.73	6.62	-	-
TiO_2-S	26.73	66.76	-	5.12	-
TiO_2-I	28.04	66.31	-	-	4.31

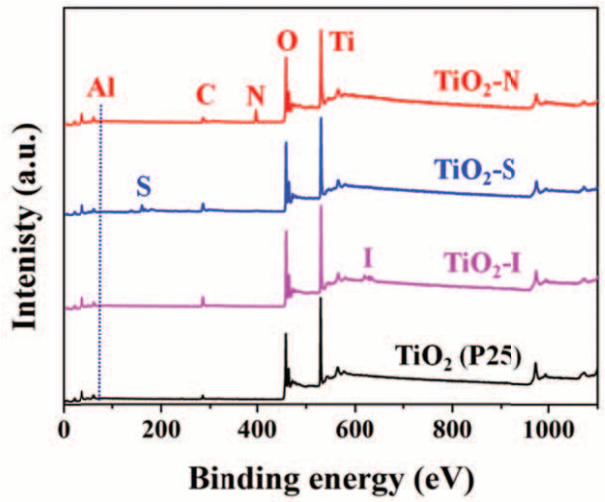

Figure S7. Full-scale XPS spectra of TiO_2-*X*.

4. The calculation of solar absoption of TiO_2-N

We obtained the absorbance of titania samples by UV-Vis-IR diffuse reflectance spectra. The solar absorption of the TiO_2-N is given by the equation:

$$A = \frac{\int (1-T)\cdot S \cdot d\lambda}{\int S \cdot d\lambda}$$

where A is the solar absorption; T is reflectance of the sample, S is solar spectral irradiance (W m^{-2} nm^{-1}), shown in Figure S8; λ is the wavelength (nm). Here, the $(1-T)\cdot S$ represents the sample absorption of solar spectral irradiance.

Therefore, we can obtained the solar absorption of the TiO_2-N was approximate 85%.

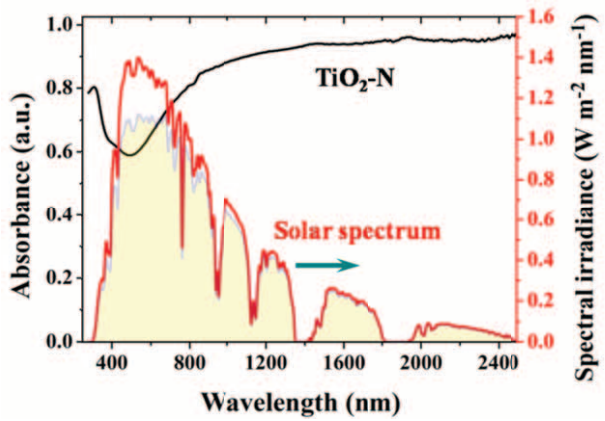

Figure S8. The absorbance of TiO_2-N (black line), solar spectral irradiance (red line, *S* in Equation 1) and TiO_2-N absorption of solar spectral irradiance (filled with canary yellow, $(1-T)\cdot S$).

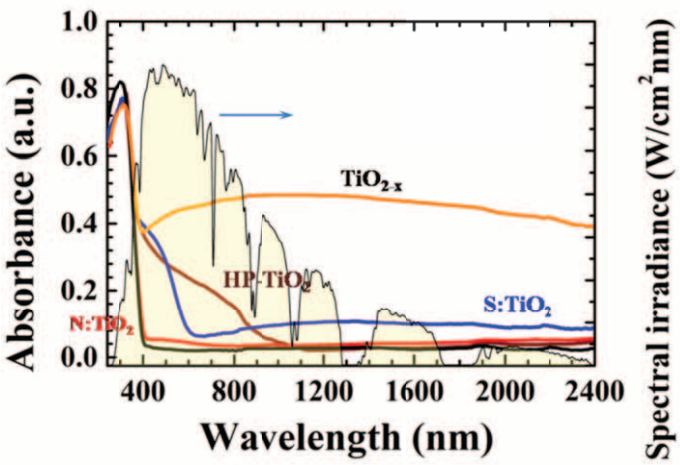

Figure S9. Diffuse reflectance spectra of pristine TiO_2; our black TiO_{2-x} prepared by Al-reduction; black titania obtained by high-pressure H_2 annealing (HP-TiO_2); N- and S-doped TiO_2 samples (N:TiO_2, S:TiO_2) following the literature preparations.

5. VB XPS and magnetic field dependence of magnetization of TiO_2-X

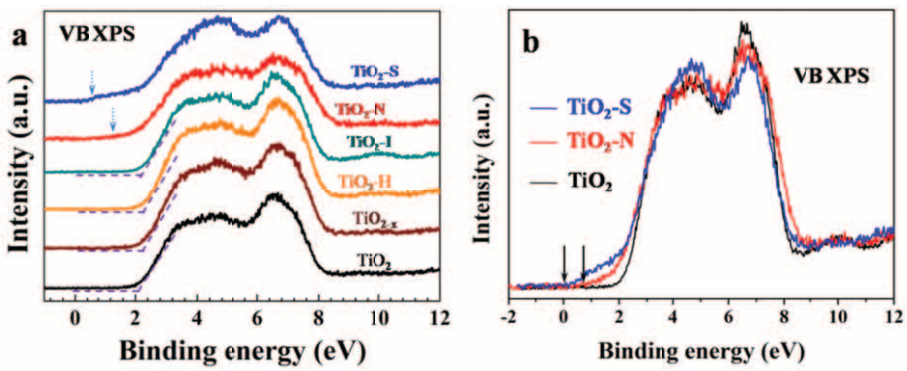

Figure S10. XPS valence band spectra of prisitine, TiO_{2-x} and TiO_2-*X* (*X* = H, N, S, I).

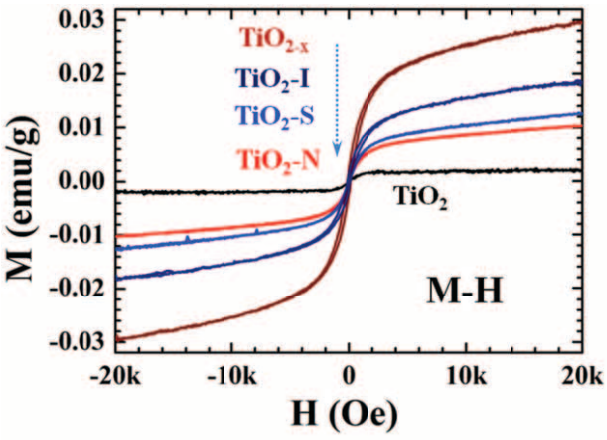

Figure S11. Magnetic field dependence of magnetization of TiO_{2-x}, TiO_2-I, TiO_2-N, TiO_2-S and pristine TiO_2.

6. Experimental details of H_2 generation

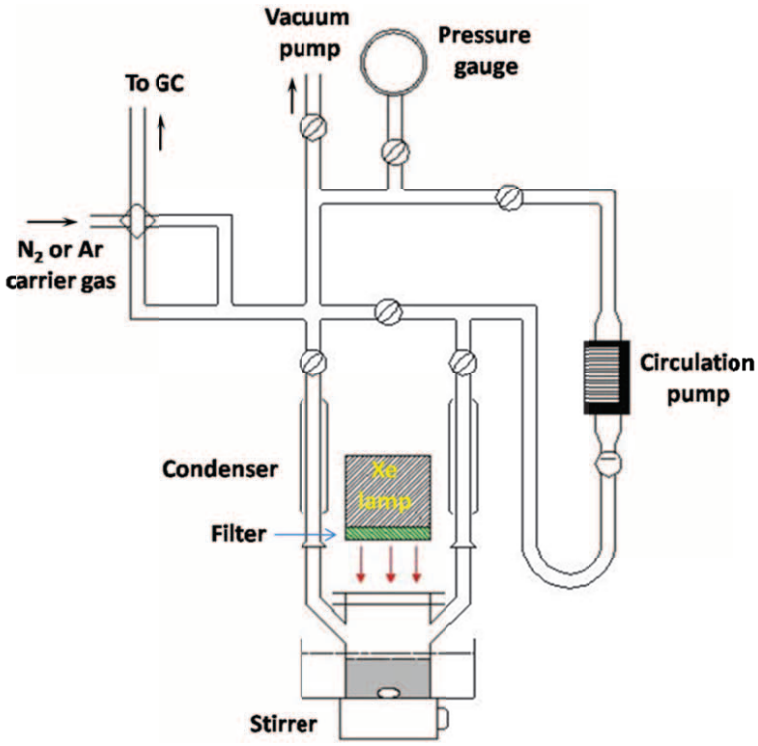

Figure S12. Experimental setup for H_2 production from water over the photocatalyst under Xe lamp irradiation and a closed gas circulation system.

Hydrogen production by photocatalytic H_2 generation was carried out in a top-irradiation Pyrex reaction cell as shown in Figure S12. 100 mg photocatalyst powder was dispersed by ultrasonic for 2 min in a 200 mL aqueous solution containing 40 mL methanol as the sacrificial reagent. 0.5% Pt were loaded in situ by impregnation 0.05 mL of H_2PtCl_6 (10 g/L) in the suspension. Then the suspension was thoroughly degassed by pure N_2 and irradiated by

a 300 W Xe lamp with 400 nm cut-on filter. This filter can cut off >99.9% UV light, confirmed by UV-vis absorption spectrum in Figure S13. The temperature of the reaction solution was maintained at room temperature by a flow of water. The evolved H_2 amount was determined using a gas chromatograph (Shanghai, GC-7900, TCD, N_2 carrier). The photocatalytic activities were compared by the average H_2 evolution rate in the first 3 h.

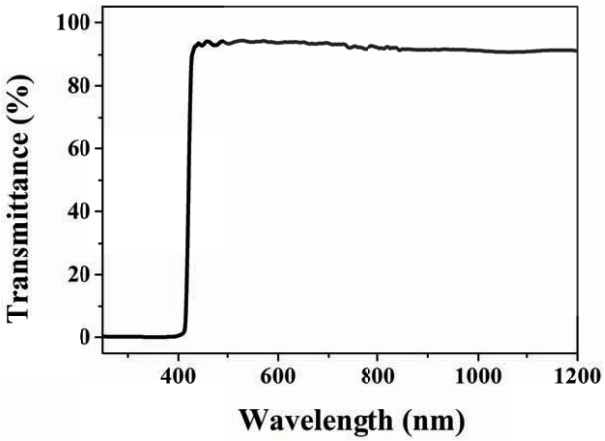

Figure S13. Transmittance of the 400 nm cut-on filter used in our research.

7. The photocatalytic activities of nonmetal-doped titania prepared by the literature methods

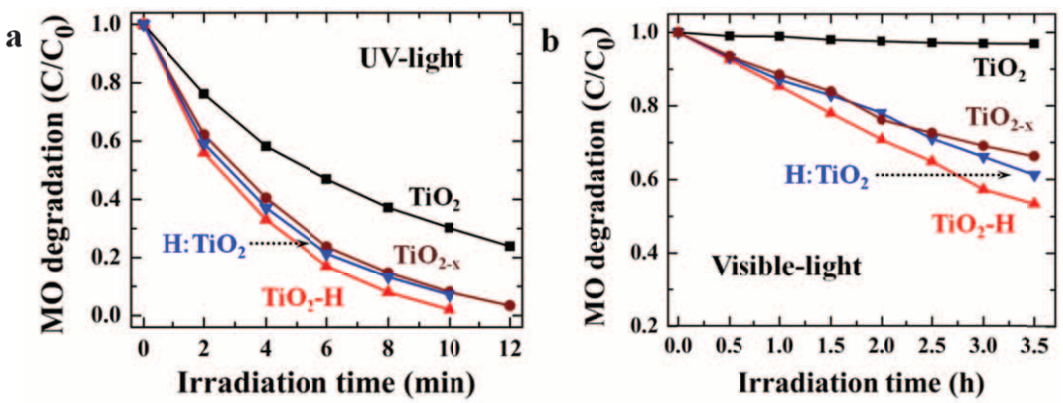

Figure S14. (a) UV-light and (b) visible-light driven decomposition of methyl orange over H-doped TiO_2 (H:TiO_2) and our TiO_2@TiO_2-H (TiO_2-H). The trend of photocatalytic activity is TiO_2-H > H:TiO_2 > TiO_2 driven by UV or visible light.

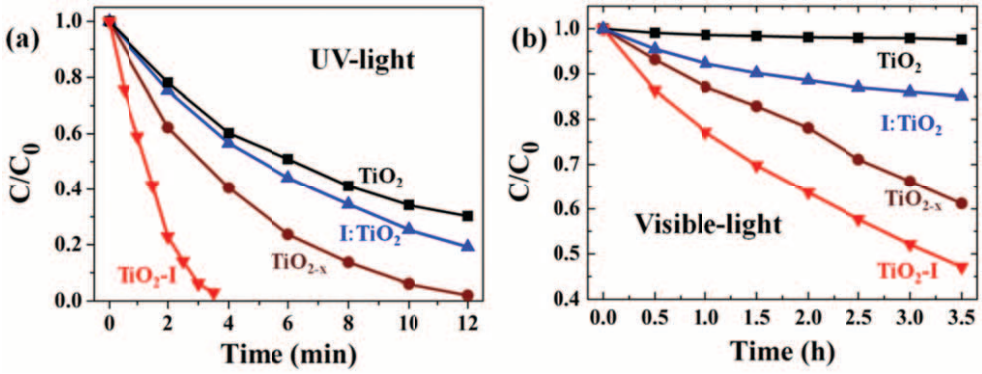

Figure S15. (a) UV-light and (b) visible-light driven decomposition of methyl orange over I-doped TiO_2 (I:TiO_2) and TiO_2@TiO_2-I (TiO_2-I). The trend of photocatalytic activity is TiO_2-I > TiO_{2-x} > I:TiO_2 > TiO_2 driven by UV or visible light.

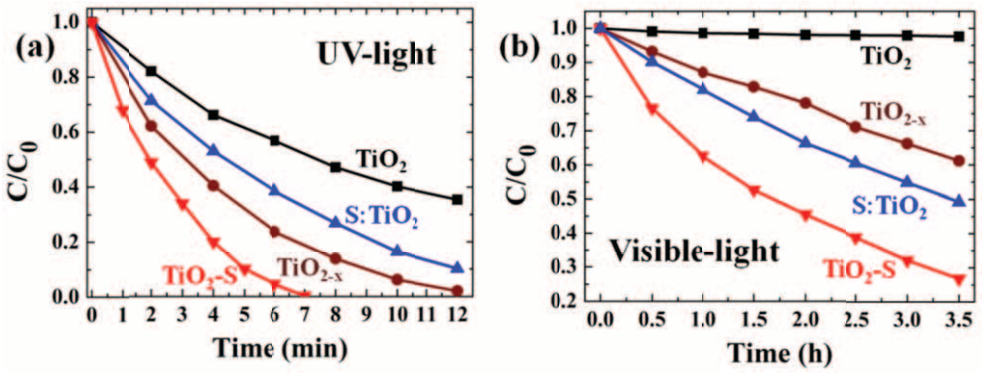

Figure S16. (a) UV-light and (b) visible-light driven decomposition of methyl orange over S-doped TiO_2 (S:TiO_2) and TiO_2@TiO_2-S (TiO_2-S). The trend of photocatalytic activity is TiO_2-S > TiO_{2-x} > S:TiO_2 > TiO_2 driven by UV light while the trend is TiO_2-S > S:TiO_2 > TiO_{2-x} > TiO_2 driven by visible light.

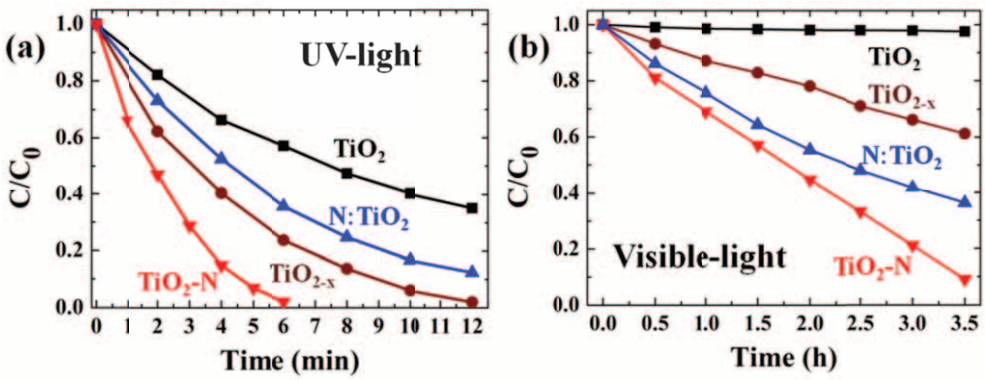

Figure S17. (a) UV-light and (b) visible-light driven decomposition of methyl orange over N-doped TiO_2 (N:TiO_2) and TiO_2@TiO_2-N (TiO_2-N). The trend of photocatalytic activity is TiO_2-N > TiO_{2-x} > N:TiO_2 > TiO_2 driven by UV light while the trend is TiO_2-N > N:TiO_2 > TiO_{2-x} > TiO_2 driven by visible light.

8. References

S1. Asahi, R.; Morikawa, T.; Ohwaki, T.; Aoki, K.; Taga, Y., *Science* **2001**, *293*, 269.

S2. Li, H.; Zhang, X.; Huo, Y.; Zhu, J., *Environ. Sci. Technol.* **2007**, *41*, 4410.

S3. Su, W.; Zhang, Y.; Li, Z.; Wu, L.; Wang, X.; Li, J.; Fu, X., *Langmuir* **2008**, *24*, 3422.

S4. Di Valentin, C.; Pacchioni, G.; Selloni, A.; Livraghi, S.; Giamello, E. *J. Phys. Chem. B* **2005**, *109*, 11414.

S5. Barolo, G.; Livraghi, S.; Chiesa, M.; Paganini, M. C.; Giamello, E. *J. Phys. Chem. C* **2012**, *116*, 20887.